Fuel 279 (2020) 118504

Contents lists available at ScienceDirect

Fuel

journal homepage: www.elsevier.com/locate/fuel

Full Length Article

Analysis of the spontaneous combustion and self-heating of almond shells

R. Font

Department of Chemical Engineering, University Institute of Chemical Process Engineering, University of Alicante, Spain

GRAPHICAL ABSTRACT

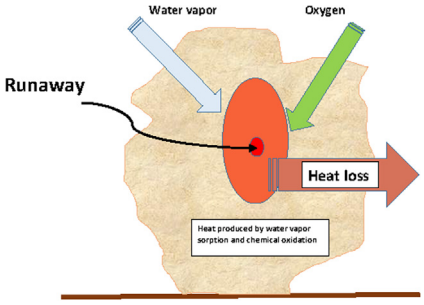

ARTICLE INFO

Keywords:
Spontaneous combustion
Self-heating
Water vapor sorption
Kinetics
Almond shells

ABSTRACT

Self-heating/spontaneous combustion of almond shells in a laboratory oven with control of temperature and weight variation was studied. Two processes were considered: water vapor sorption and chemical oxidation. Different runs were made to analyze the vapor sorption at different oven temperatures, measuring weight gain due to sorption and the variation in internal temperature. With respect to oxidation kinetics, three studies were carried out: the rate of weight variation with temperature, the variation of temperature in a runaway test carried out with a spherical sample wrapped in perforated aluminum foil, and a series of runs to analyze temperatures within spherical samples.

A simulation program was developed for the analysis of the sorption run and the kinetic run. In addition, the simulation program was used for the expected runaway condition for a 3–4 m diameter body, discussing the influence of the presence of water vapor.

1. Introduction

Spontaneous combustion or self-ignition has been considered by different authors in the literature. In the self-heating process, there is an increase in temperature, and when this increase is very high the material is ignited; this process is called spontaneous combustion.

The study of the self-heating process is very important in many industries, as large amounts of solids are stored inside silos or heaps outdoors or inside warehouses. It can also be important in forests, where there may be an accumulation of organic material of different origins.

Different mechanisms can be distinguished in the processes of self-heating: aerobic digestion, water vapor sorption and chemical oxidation.

Aerobic digestion of different wastes is carried out by different microorganisms and can lead to a rise in temperature from room temperature to 60–75 °C. Sorption of water vapor in a dry solid can cause an increase of 30–50 °C or more. By chemical oxidation of dry or wet solids, the temperature can rise above 220–240 °C with consequent onset of spontaneous combustion.

Aerobic fermentation requires carbon to produce energy, nitrogen for the generation of more microorganisms, atmospheric oxygen to

E-mail address: rafael.font@ua.es.

https://doi.org/10.1016/j.fuel.2020.118504
Received 7 February 2020; Received in revised form 19 June 2020; Accepted 20 June 2020

Table 1
Water vapor sorption.

Material	Process/apparatus	Description	Authors and year	Ref.
Refuse-derived fuel and meat bone meal	Calorimeter, Dewar vessel	The temperature can rise more than 30–56 °C	Fu et al. (2006)	[1]
Jute, flax, coir, cotton, hemp, sitka spruce	Dynamic vapor sorption apparatus	The moisture content increases to 15–30% at an air humidity close to 95%	Hill et al. (2009)	[2]
Cellulose nanocrystals and nanofibers	Dynamic vapor sorption apparatus	The equilibrium moisture range is 21–39% at a relative humidity of 95% at 6.5–43 °C	Guo et al. (2017)	[3]
Henna leaves	Dynamic vapor sorption apparatus	Sorption isotherms at 30, 40 and 50 °C and kinetics	Sghaier et al. (2017)	[4]
Grained wood at low relative humidity	Water vapor sorption runs	Sorption kinetics	Murr and Lackner (2018)	[5]

oxidize the material and moisture of around 40–60% to maintain the aerobic fermentation process. The phases of the exothermic aerobic process are the following: an initial rise from room temperature to 40–50 °C in the mesophilic range (1–2 days), a second rise to 60–75 °C in the thermophilic range (3–5 days) and a maturation process (3 or 4 weeks) in the mesophilic range (40 °C to room temperature). Carbon dioxide, ammonia and water are the main products of the fermentation process. The literature on this process is very extensive, and some papers referred to herein consider the characteristics of the process.

Many references have analyzed the self-heating of biomass materials due to the sorption of water vapor. This self-heating can be an intermediate step in the ignition of the solid. Table 1 shows some references on different aspects of the sorption process of biomass samples: equilibrium data, kinetics of the vapor sorption process and temperature increase:

With respect to chemical oxidation, it has been observed that there are many interesting references to the oxidation of coal, so both coal and biomass oxidation papers have been reviewed. In the initial characterization of the solids for chemical oxidation, different parameters and analyses can be studied: composition, elemental analysis, proximate analysis, net calorific value (NCV), the Maciejasz Index, the emission temperature of flammable volatile compounds different types of thermal analysis, minimum ignition temperature of a dust layer, etc.

Many authors have analyzed self-ignition considering the Frank-Kamenetskii theory of criticality [6,7]. This theory was developed for thermal explosion and is based on some considerations: evolution of heat with the Arrhenius equation rate, heat loss assuming that the external temperature coincides with the ambient temperature, and the internal heat transfer of Fourieŕs law. Depending on the ambient temperature, the system can reach a pseudo-stationary state below the ignition point where the heat generated is equal to the heat lost. Above a critical ambient temperature, the heat generated is greater than the heat lost, and the temperature of the solid increases continuously and the ignition process takes place.

The critical behavior for an ambient temperature $T_{a,critical}$ (K), also called the self-ignition temperature (SIT), which leads to spontaneous combustion, can be expressed as:

$$\delta_{critical} = \frac{\Delta H_{ox} E_{ox} r^2 k_{ox} \rho_s}{k_{eff} R T_{a,critical}^2} \exp\left(-\frac{E_{ox}}{R T_{a,critical}}\right) \quad (1)$$

The critical dimensionless parameter $\delta_{critical}$ takes the value of 3.32 for a sphere. The parameter r is the radius of the sphere (m), ΔH_{ox} is the heat of reaction (J/kg), E_{ox} is the activation energy (J/kmol), k_{ox} is the pre-exponential factor of the chemical reaction rate (s^{-1}), k_{eff} is the thermal conductivity (J/s m K) and R is the gas constant (J/kg K).

From the previous equation, it can be deduced that

$$\ln\left[\frac{\delta_{critical} T_{a,critical}^2}{r^2}\right] = \ln\left[\frac{\Delta H_{ox} E_{ox} k_{ox} \rho_s}{R k_{eff}}\right] - \frac{E_{ox}}{R T_{a,critical}} \quad (2)$$

The EN15188 test method considers different volumes in an isothermal oven. Taking into account the previous equation or a similar equation with the volume/external surface ratio, it is possible to estimate the critical ambient temperature for large-scale solids from experimental values obtained with small laboratory-size samples. In some cases, the parameter of length such as the radius r can be related to the volume/external area ratio of different body types.

Oxidation kinetics can also be obtained from an adiabatic hot-storage test [8]. The oven is controlled to increase its temperature T and keep it the same as the material inside the basket, which increases due to exothermic oxidation of the material. In this case, the kinetic parameters can be obtained from the following equation, deduced for an adiabatic reactor:

$$\ln\left(\frac{dT}{dt}\right) = \ln\left(\frac{\Delta H_{ox} k_{ox}}{C_p}\right) - \frac{E_{ox}}{R}\frac{1}{T} \quad (3)$$

Table 2
Spontaneous combustion of coal samples.

Material	Process/Apparatus	Description	Authors and year	Ref.
Coal	Chamber holding 13 short tons	Analysis of reactivity, particle size, freshness, heat-of-wetting effect and oxygen	Smith et al. (1991)	[11]
Sub-bituminous coal	Adiabatic device with pure oxygen	Analysis of moisture content effect	Vance et al. (1996)	[12]
Stockpiled coals	FT-IR	Decrease in aliphatic hydrogen content and increase in carboxylic groups	Ibarra and Miranda (1996)	[13]
Seven different coals	Crossing-point method	Analysis of the activation energy and $\Delta H_{ox}k_{ox}$ and the risk of spontaneous combustion	Nugroho et al. (2000)	[14]
Coal	Two-column micro gas chromatograph	Analysis of the behavior of the oxygenated complexes and mechanism of the oxidation of coal below 100 °C,	Wang et al. (2003)	[15]
Lignite coals	Pouring water on the solids and steam injection into the oven	Analysis of the influence of wetting, which can turn a sub-critical point into a super-critical point leading to ignition	Lohrer et al. (2005)	[16,17]
Coal	Molecular-mechanics methods	Proposal of a mechanism for the initial stage with oxygen, water, hydrogen and active carbon centers	Butakova et al. (2011)	[18]
Coal dust	Hot-oven, hot plate tests and a novel basket coupled with a TG scale and FTIR spectrometer for gas analysis	Analysis of the increasing tendency for self-ignition with the increase of oxygen and carbon dioxide. Comparison of extrapolation methods. Extrapolation of critical temperature and induction time around 30–300 days (for critical temperature 20–40 °C)	Wu et al. (2015, 2017 a, b, 2019)	[19–21]
4543 Coal quality data	Correlation paper	Proposal of a quantitative coal rank scale system for predicting the self-heating temperature	Wang and Luo (2015)	[22]
Coal stockpiles	Numerical study	Effects of the wind barriers and closed storage	Kim and Sohn (2016)	[23]
Coal oxidation	Numerical study	Proposal of a modified method for obtaining the kinetic constants considering temperature profiles	Kaminsky el al. (2017)	[24]
Coal	Mathematical simulations	Analysis of the air velocity range with a high possibility of self-ignition	Lin et al. (2017)	[25]
Four types of coal samples	New method with constant temperature difference between ambient and sample	Adiabatic oxidation curves for comparison of samples	Lu et al. (2017)	[26]
Carbon-rich solids	Method similar to EN15188	Prediction of the self-ignition in different conditions of temperatures and soil layer thickness. Activation energy E_{ox} = 105–132 kJ/mol. Extrapolation of critical temperature	Restuccia et al. (2017)	[27]
Coal	Laboratory wire-mesh baskets (15–1000 cm^3) and wire-mesh basket (0.015–1 $m^{3)}$	Validation of the Frank-Kamenetskii model. Activation energy E_{ox} = 139 kJ/mol. Extrapolation of critical temperature and induction time to 365 days (for critical temperature 38 °C)	Wang et al. (2017)	[28]
Accumulated peat dusts	Combustion chamber with dust sample in a basket	Effects of the thickness, grain size, and acidity	Polka (2018)	[29]
Coals of different origins.	Hot plate and oven-basket	Computational model	Yuan et al. (2019)	[30]

Table 3
Spontaneous combustion of coal and biomass samples.

Material	Process/Apparatus	Description	Authors and year	Ref.
Dusts: coal, activated carbon, zinc powder and several biomass samples	Dust layer on hot surface and EN 15188 method	Satisfactory correlation for determination of self-ignition by the two methods	Janes et al. (2008)	[31]
Lignite coal, pine wood chips	Mathematical model with biological process, sorption and chemical oxidation	Validation of experimental data at small scale and computation of a real-scale smoldering fire scenario. Simulation time to 4 years in coal seams. Ignition time in a pile of wood chips around 300 days (ambient temperature 15 °C)	Krause et al. (2009)	[32]
Coals, sewage sludge and other biomass materials	EN 15188 method	Determination of risk. Extrapolation of critical temperature and induction time. Critical storage time for sewage sludge of 100–1000 days for temperatures 55–30 °C	García-Torrent et al. (2012)	[33]
Lignite coal, black coal, cork dust, polymer dust, silicid acid	Adiabatic hot-storage tests and EN 15188 method	Similar kinetic parameters for both methods. Determination of pre-exponential factors and activation energy E_{ox} = 85–105 kJ/mol	Schmidt et al. (2013)	[8]
Bituminous and brown coals, wood pellets and sawdust	EN 15188 method	Analysis of parameters for safe storage	Veznikova et al. (2014)	[34]
Different types of coal	EN 15188 method, Simultaneous thermal analysis (TG + DSC) with FTIR	Influence of inert additives. Activation energy 57–122 kJ/mol	Binkau et al. (2015)	[35]
Coals of different rank	TGA	Prediction of the ignition temperature and spontaneous combustion propensity	van Graan and Bunt (2016)	[36]
Lignite coals, almond shells and olive residue	TGA/DSC tests and an entrained flow reactor coupled with an imaging system to observe the ignition of single particles	Analysis of the ignition	Magalhaes et al. (2017)	[37]
Bulk fuels: coal, sewage sludge, wood and other biomass	Hot surface equipment to determine minimum ignition temperature	Study of the influence of particle size and density	Fernandez-Anez et al. (2019)	[38]

Table 4
Spontaneous combustion of compost and sewage sludge.

Material	Process/Apparatus	Description	Authors and year	Ref.
Composting of cellulosic material	Simulation of the increase of temperature due to microorganisms and oxidation process	Analysis of different behaviors and critical points	Sidhu et al. (2007)	[39]
Composting of sewage sludge	Numerical simulation taking also into account the heat generation by microorganisms	Influence of the height pile (below 1.8 m there is no ignition). Induction times considering the biological process greater than 200 days	Moraga et al. (2009)	[40]
Sewage sludge	TG/DSC, thermal stability, tests for transportation or storage of large quantities were done carried out in oven a 140 °C for 24 h	Knowledge of ignition properties. Extrapolation of critical temperature and induction time to 3 years for ambient temperature 62 °C	Pejic et al. (2015)	[41]
Sewage sludge and several biomass types	Flammability, explosibility, thermal susceptibility	Positive influence of the H/C ratio to ignition	García-Torrent et al. (2016)	[42]
Composting of sewage sludge	Mathematical model considering moisture transfer, heat, the biological activity and chemical oxidation	Spatial profiles of temperature, oxygen and moisture. Long periods of time 46–100 weeks, considering biological process	Putranto and Chen (2017)	[43]
Sewage sludge	TG	Susceptibility to self-ignition considering the Maciejasz Index, some TG parameters cited previously, chemical composition and combustion enthalpy	Diaz et al. (2019)	[44]

Table 5
Spontaneous combustion of other biomass samples.

Material	Process/Apparatus	Description	Authors and year	Ref.
Dairy powders	Crossing-point temperature at the center	Analysis of the values $\Delta H_{ox}k_{ox}$ and activation energy E_{ox} 75–97 kJ/mol	Chong et al. (1999)	[10]
Wood piles	EN 15188, respirometric tests and large-scale experiments in wood piles	Mathematical model for testing model and predictions. Simulation data to 309 days (ambient temperature 15 °C)	Ferrero et al. (2009)	[45]
Solid wastes from a landfill	Dynamic runs carried out in an oven, measuring temperatures at the surface and at the center of the sample	Study of the incidence of the moisture, oxygen concentration and leachate components on self-ignition	Moqbel et al. (2010)	[46]
Dusts of icing sugar, flour, maize, wheat, barley, alfalfa and soybean,	Maciejasz index, the emission of flammable volatile compounds, characteristic temperature with oxygen, DSC analysis, method EN15188	Provide information for thermal susceptibility to ignition and for silo design. Assuming Semenov for wheat dust, the deduced induction time is 14 years for ambient temperature 65 °C	Ramirez et al. (2010)	[47]
Several biomass samples	TG, DSC	Determination of self-ignition risk in storage	García-Torrent et al. (2015)	[48]
Different biomass fuels	Two sensitive heat-flux calorimeters, one of them to measure the activity of microorganisms	Moisture increases the heat evolved	Murasawa and Koseki (2015)	[49]
Seven biomass fuels	STA, single particle combustion and dust layer experiments, TGA-FTIR	Analysis of the ignition tendency, based on the kinetic parameters	Jones et al. (2015)	[50]
Pine bark	Oxidant atmosphere	Influence of oxygen content	Ronda et al. (2017)	[51]
Wood pellets	Isothermal calorimetry, oxi-press and TGA, VOC, off-gassing tests, Soxhlet extraction	Correlation between self-heating tests and off-gassing tests	Sedlmayer et al. (2018)	[52]
Wood pellets and four biomass samples	TG	Kinetic parameters for low temperature pyrolysis and oxidation	Schwarzer et al. (2019)	[53]

where C_p (J/s m K) is the specific heat capacity of the solid.

The Chen and Chon [9] method consists of heating a small sample inside an oven at a constant heating rate and determining the external temperature and the temperature inside the sample, the crossing-point temperature being when the internal temperature coincides with and afterwards exceeds the external temperature. Another method consists of measuring the temperature at the center and at another point close to the center, and the ambient temperature in the oven. When the temperatures at the center and at a point close to the center of the body are the same (crossing-point temperature), the heat developed by the oxidation reaction is equal to the variation in temperature, and an equation similar to (3) is deduced [10].

In the Semenov (well-stirred) theory, it is assumed that the temperature is uniform within the body, and the only heat transfer to be considered is from the external surface to the ambient [7].

Different ovens and configurations have been used to study the ignition process. These apparatuses and procedures are described in the analysis of the contributions of different researchers.

Tables 2–5 present some interesting contributions to the self-heating process for coal (Table 2), for coal and biomass (Table 3), for compost and sewage sludge (Table 4) and for other biomass samples (Table 5). The reason for classifying these contributions is for comparison of the papers, which are ordered by publication date.

The objective of this work has been to study the sorption of water vapor and chemical oxidation of almond shells by new procedures. Almond shells were selected because is a solid fuel that can undergo self-heating and there is evidence that some spontaneous combustion incidents have occurred. Two methods have been developed to study the self-heating that can lead to the spontaneous combustion in large piles, and in addition a simulation program is presented to test the experimental results and for the analysis of the two processes.

2. Material and methods

2.1. Material

The material used was almond shells, mainly of the marcona variety obtained from the cracking process, with 67% of size greater than 13 mm. Table 6 shows the chemical/physical characterization of the material used.

Elemental analysis, determined with Perkin-Elmer 2400 apparatus, and the NCV determined using AC-350 LECO calorimetric bomb, are shown in Table 6. Oxygen and inorganic compounds have a percentage of 40.6 (calculated as difference between 100 and the percentages of carbon, hydrogen, nitrogen and ash). Ash content was determined by an oven at 550 °C.

The specific heat value was determined by the hot water process in an adiabatic vessel; the determined value is close to that proposed by Dupont et al. [54].

2.2. Apparatus

Fig. 1 shows the apparatus used. Inside the laboratory oven, a sample of about 4–10 cm diameter was placed inside a spherical foil above a small rack or on a plate to record the variation in weight using an external balance. The foil was used to hold the sample and form a

Table 6
Characterization of almond shells.

Elemental analysis (dry basis)		Bulk properties	
C	51.2	Density	361.6 kg/m^3
H	6.5	Specific heat	1435 J/kg K
N	0.2	Thermal bulk conductivity	0.120 J/s m K
O	40.6 (by difference)	NCV	18.29 MJ/kg
Ash	1.5		

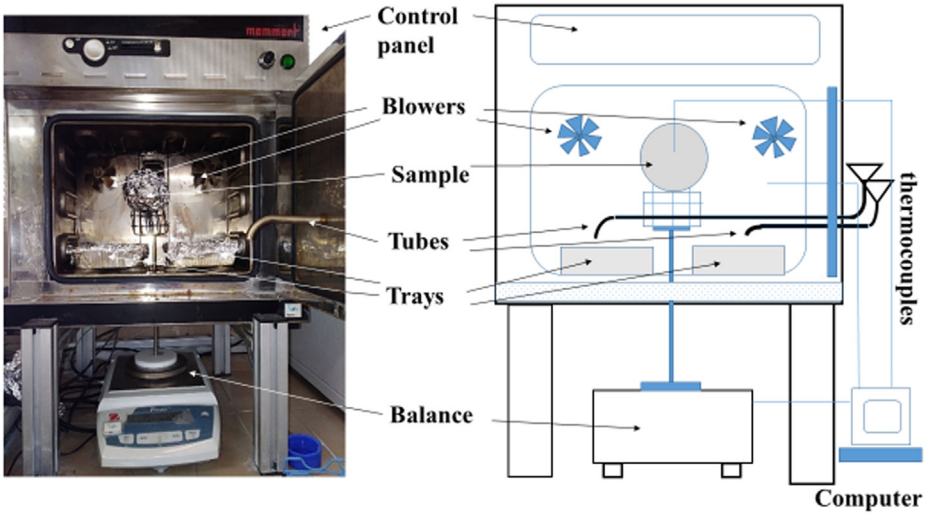

Fig. 1. Apparatus used: furnace, blowers, aluminum foil trays, balance.

sphere. Drilling was manual with at least 4 holes/cm^2, with a hole diameter of around 1 mm. It was proven that vapor and oxygen could transfer without a significant resistance. On the sidewall in front of the oven door there were two small blowers to circulate the internal atmosphere with a controlled turning speed. At the bottom, there were two aluminum foil trays to collect the introduced hot water directly into them or through two curved tubes in some runs. The water was vaporized immediately after adding hot water 10–15 °C above the nominal temperature inside the oven to obtain an almost saturated environment during the first part of the run, and then in equilibrium with water with 10–15 °C below the nominal temperature of the oven. The pseudo-equilibrium moisture of the almond shells was tested to depend mainly on the oven temperature. The temperature of the oven increases 2–3 °C during a short period of time above the nominal temperature as a consequence of the hot water and of the heat evolved due to sorption.

At least two thermocouples K were used, one placed with the tip approximately at the center of the spherical body, and another outside the spherical body to record the ambient temperature. Sometimes a third thermocouple K was used to measure the temperature at different parts of the oven or inside the sample. Temperatures were continuously registered with units of degrees Celsius, although in some cases the temperature was considered with a precision of 0.5 °C when it ranged between two consecutive values.

Weight and temperatures were recorded continuously every 10 s.

2.3. Method

With the oven as explained above, five types of run were carried out:

a) The determination of the heat transfer coefficient. For each size, a spherical ball made with pieces of wet filter paper wrapped in a perforated foil was introduced. From the weight loss due the vaporization of the water and the temperatures inside and outside the spherical ball, the heat transfer coefficient was calculated. The run was repeated at different temperatures to test the values obtained.
b) A second type of run was performed to obtain the value of the thermal conductivity of the dried sample of almond shells. The sample was wrapped in a non-perforated foil, but with an open hole in the upper part of the spherical body. This sphere was introduced into the oven and dried until constant weight, at about 120 °C. The oven was then opened and the upper hole closed, maintaining the temperature of the oven constant at around 40 °C. The variation in the temperature recorded by the thermocouple whose end was approximately at the center of the sphere was recorded vs. time, and from this variation the thermal conductivity was calculated.
c) A third type of run was performed to obtain the increase in weight of the dried sample within a plate that transmits its weight to the balance. In some runs, a spherical sample of almond shells was wrapped in aluminum foil, forming a spherical body, and the external foil perforated with small holes for the flow of water vapor and oxygen. In both types of run, when the sample reached a steady state with constant weight or with a very small variation, hot water was introduced into the oven by means of the two curved tubes that discharged the hot water into the aluminum foil trays. The water vapor evolved inside the oven maintained an atmosphere with a high concentration of water vapor. In the spherical body, there was an increase in temperature within the sample.
d) A fourth type of run was performed to determine the weight loss due to the chemical oxidation of the material, in a dry atmosphere or in the presence of water vapor, and with samples inside a plate or formed into a spherical body in perforated aluminum foil (in these runs, the internal temperature was also recorded).
e) The final type of run was carried out to determine the temperature in the center of the sphere after reaching steady conditions and observing whether the temperature increased continuously up to 190–200 °C, indicating a runaway.

2.4. Simulation program for water vapor sorption and chemical decomposition.

A simulation program was prepared to discuss the experimental results and to extrapolate under various conditions. The program was an adaptation of the process from a previous study for the study of sewage sludge drying [55]. The spherical body was divided into 20 vol elements with the same dry solid mass. The equations corresponding to the mass and energy balances were deducted and applied to each element, taking into account the mass and heat flows and the heat developed due to sorption of water vapor. Excel spreadsheets were used to simulate the process, and the program was tested with the analytical solutions obtained in many different cases.

The following equation was used for external mass transfer:

$$N_w = K_X(X_a - X_{eq})A_s \quad (4)$$

where N_W (kg water/s m^2) is the flow of water vapor from the ambient to the external surface of the spherical body, K_X (kg water/s m^2 Δ(kg water/kg dry air)) is the mass transfer coefficient, X_a is the humidity of the surrounding air (kg water/kg dry air), X_{eq} (kg water/kg dry air) is

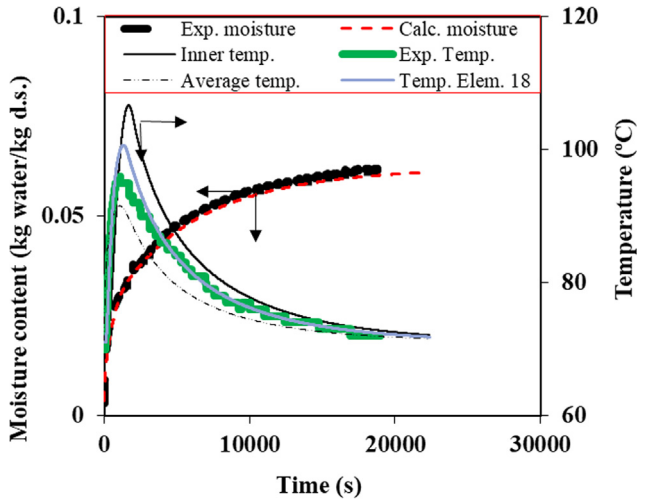

Fig. 2. Sorption run at low temperature (70 °C) in a foil sphere: experimental and calculated values.

the humidity equilibrium of the external volume element with the water content and A_S (m^2) is the external surface area of the body. Humidity X_a of the surrounding air was calculated assuming that air is saturated with water according to the Antoine equation, which relates the water vapor pressure to the temperature the water introduced into the aluminum foil trays in the oven. The same results were obtained using the Clausius-Clapeyron equation with constant vaporization latent heat (value at 100 °C).

The heat transfer from the ambient to the body can be by convection and radiation, but only an overall heat coefficient h is considered:

$$Q = hA_s(T_a - T_{s)} \tag{5}$$

where Q is the heat flux (J/s) from ambient to the external sphere surface, A_s is the external surface area and T_a and T_s are the temperatures of ambient air and body surface, respectively.

Internal mass transfer is considered by the following equation:

$$\frac{\Delta M}{\Delta t} = -\frac{1}{4\pi r^2}\frac{\Delta\left[-(D_{eff}\rho_s)4\pi r^2\frac{\Delta M}{\Delta r}\right]}{\Delta r} \tag{6}$$

where ρ_s is the concentration of solids within the spherical body or the bulk density, $4\pi r^2\rho_s\Delta r$ is the mass increment of dry solids for simulation and D_{eff} (kg/m s) is the effective diffusivity of moisture within the body.

For the internal heat transfer, from the energy balance applied to an elemental volume, and assuming that the sorption of water vapor takes place within the body and not only on the surface, the following expression is deduced:

$$\frac{1}{r^2}\frac{\Delta\left(-k_{eff}\frac{\Delta T}{\Delta r}r^2\right)}{\Delta r} + \rho_S(C_{pS} + MC_{pw})\frac{\Delta T}{\Delta t} = \rho_S\frac{\Delta M}{\Delta t}r_W + \rho_S k_{ox}\exp\left[-\frac{E_{ox}}{RT}\right]\Delta H_{ox} \tag{7}$$

where k_{eff} (J/s m K) is the effective thermal conductivity within the body, C_{ps} and C_{pW} are the specific heats of the solid and the liquid water (4180 J/kg K), respectively, and r_W (J/kg) is the enthalpy of vaporization of water.

The vaporization enthalpy r_W was calculated by the Regnault equation:

$$r_W\left(\frac{J}{kg}\right) = 2\ 540,\ 000 - 2910T(^oC) \tag{8}$$

3. Results and discussion

3.1. Determination of heat transfer coefficient

Following the procedure described above, 4- and 9-cm diameter spheres were prepared with wet paper inside the spheres until a steady constant temperature was reached inside each. Constant weight loss due to the vaporization of water was measured and considering the water enthalpy calculated at the internal temperature, the heat transfer coefficient was calculated. The external temperature was 70–120 °C and the internal temperature was 50–80 °C. The heat transfer coefficients, taking into account the external resistance and the aluminum wall were 21.2 and 11.5 J/s m^2 K for the 4- and 9-cm diameter spheres, respectively.

3.2. Determination of thermal conductivity

A spherical body of approximately 10 cm diameter was prepared, containing the material wrapped in non-perforated aluminum foil, and following the proposed procedure the internal and external temperature were recorded. Using the simulation program obtained previously, the thermal conductivity value was calculated taking into account the value of heat transfer coefficient previously deduced. The external temperature was 42 °C and the internal temperature fell from the initial 120 °C to a final temperature of 42 °C. The estimated value was 0.120 J/s m K, so the calculated variation of the internal temperature is nearly coincident with the experimental variation.

3.3. Analysis of vapor sorption

Two types of runs were made: some using samples of almond shells wrapped in perforated aluminum foil to study the kinetics of sorption and others in samples of almond shells in small open aluminum foil trays.

Fig. 2 shows the experimental results of a run with almond shells inside a 9.2 cm diameter spherical body at 70 °C, observing the increase in moisture content after the addition of hot water at around 85 °C to the aluminum foil trays and also the temperature of the thermocouple sited near the center of the body. The temperature of the water inside the aluminum foil trays decreases rapidly to around 75 °C, and then decreases slowly to 65–55 °C. Both the water content and the temperature increased very rapidly at the beginning of the run, and then the moisture adsorption rate decreased and the temperature at the center also decreased. After the analysis carried out by testing different simulation models, it was concluded that at the beginning of the run the solid reached pseudo-equilibrium conditions for a period of time controlled by the sorption kinetics. Subsequently, the sample was cooled, because the sample temperature was higher than that of ambient, and in accordance with the sorption equilibrium, more moisture was adsorbed, so the moisture content increased. The pseudo-equilibrium moisture content for a high water vapor concentration ambient (obtained from water around 55–75 °C inside the aluminum trays) was determined when the internal temperature of the sample was equal to the oven temperature and the rate of increase in moisture content was very small. By the analysis carried out to the non-isothermal sorption, the evolution of the moisture content shown in Fig. 2 is consistent with pseudo-equilibrium data that are presented below. The diameter was deduced from the mass of the sample and its density, which was very close to that measured.

Fig. 3 shows another run carried out at high temperature for the determination of the vapor sorption equilibrium and with the determination of the weight loss kinetics due to chemical oxidation. For the runs carried out above 100 °C, hot water was added and the temperature of the water was around 75–85 °C.The run of Fig. 3 used a 56 g sample placed in an aluminum foil tray. Different sections can be observed when plotting the ratio kg water + kg dried solid/initial dried

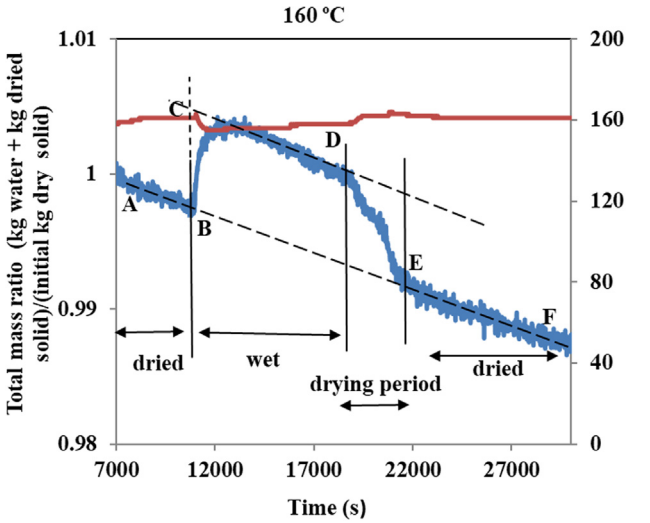

Fig. 3. Sorption run at high temperature (160 °C) in a foil sphere: experimental and calculated values.

solid vs. time. The variation of sections AB and CD correspond to a decrease due to chemical oxidation, whereas the increase in intermediate sections corresponds to the period of time when hot water was added and water vapor was present inside the oven. The equilibrium data correspond to the difference between the B and C values. It can be seen that chemical decomposition also takes place in the vapor/air atmosphere.

For different oven temperatures, Fig. 4 shows the moisture content corresponding to the vapor in equilibrium with the vapor generated from the hot water at 65–85 °C inside the aluminum foil trays for the runs with upper temperature higher than 70 °C and with water at the same temperature as the oven when the temperature is less than 70 °C. The upper part shows the variation over a wide temperature range and the lower part only over the interval used for simulation of the data shown in Fig. 2, although the difference between the variations deduced are small.

Fig. 2 also shows the simulated results of the experimental data for the run carried out at 70 °C, both the variation of the moisture of the sample and the internal temperature in two elements: the center of the body or element 20 and the adjacent to the adjacent to the center or element 18. The values of the mass transfer coefficient and thermal conductivity were those deduced previously. The heat transfer coefficient and the effective diffusivity were selected to obtain an acceptable fitting of the experimental data, with the values K_x 0.008321 kg water/s m^2 Δkg water/kg air, and effective diffusivity 1.575 × 10^{-7} m^2/s. However, the value of K_x was close to that deduced from the test performed to determine the heat transfer coefficient, and the effectivity diffusivity was also close to that deduced by applying the King model for sorption and desorption [56].

Note that for the temperature, the thermocouple measures the temperature inside the air space close to the center of the sphere and there may be a small difference in the observed peak temperature between the actual temperature of the solid and the air. The discrepancies may also be due to the proposed approximate model and the physical parameters.

3.4. Kinetics of the process

The weight loss due to chemical oxidation was determined with samples in the spherical body or in small trays from 50 to 200 g during a prolonged period sufficient to obtain a significant value of weight variation. Fig. 5 shows the variation in weight loss from the initial weight with and without water vapor at different temperatures.

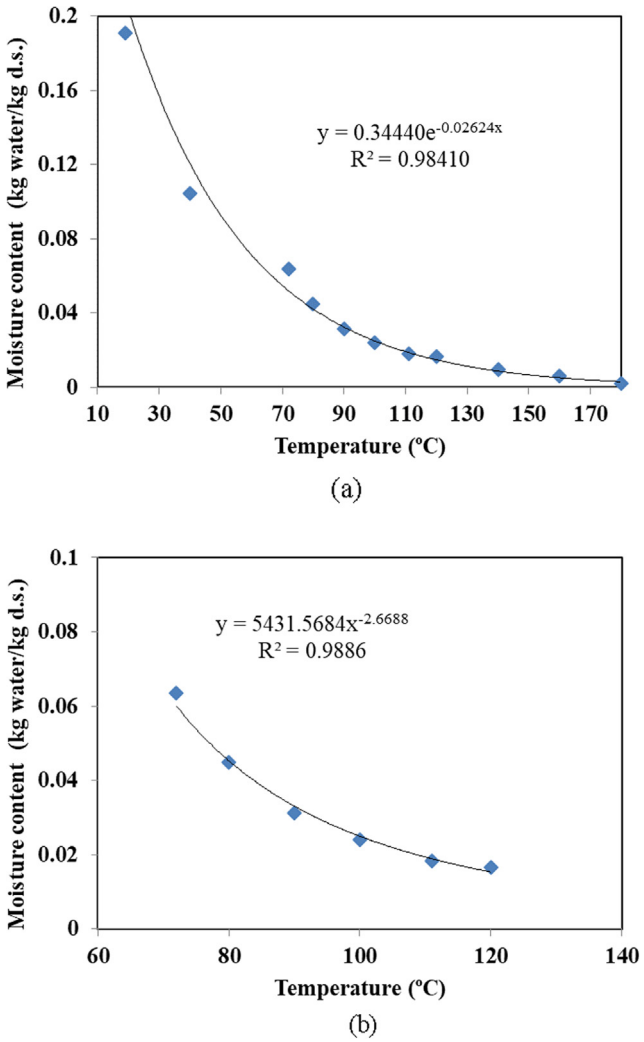

Fig. 4. Sorption data as a function of oven temperature with vapor generated with hot water at 65–85 °C.

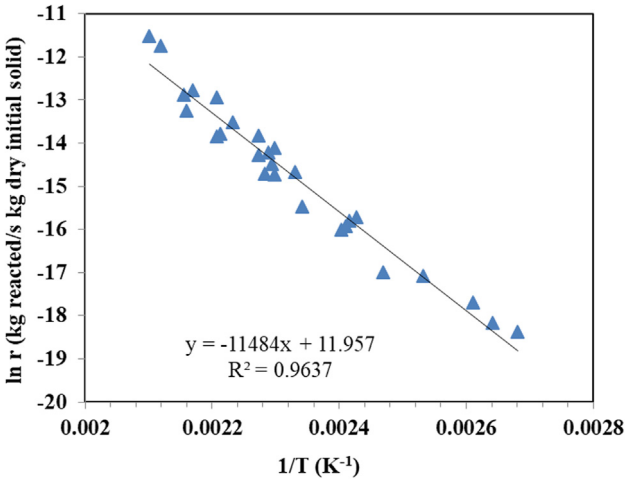

Fig. 5. Variation of the reaction rate vs. absolute temperature inverse.

Fig. 6 shows the experimental results of a runaway run, with the 10 cm in diameter spherical dried sample with perforated aluminum foil. The simulated results were obtained with the values of C_{ps}, h, k_{eff} obtained previously, the Arrhenius variation observed in Fig. 5, and an enthalpy reaction of 5.214 × 10^6 J/kg (around 28.5% of the NCV). A

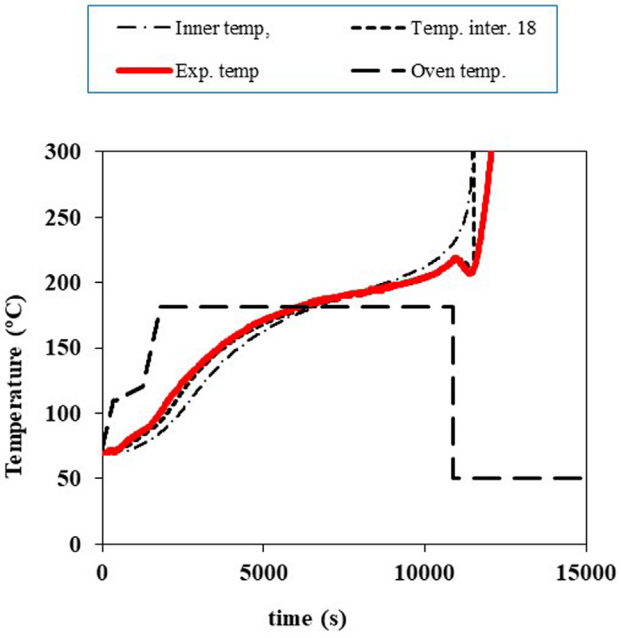

Fig. 6. Variation of temperature vs. time for a runaway run.

good fitting can be observed considering the variation in element 18 close to the center of the sphere. Be aware that the thermocouple measures the temperature of the air around its tip, which also transfers heat through the metal thermocouple.

3.5. Self-heating analysis considering maximum temperature increase

The following analysis has been proposed for the self-heating in a spherical body. In a run without runaway, the spherical body after a long period reaches a steady state with a temperature gradient between the outer surface and the center of the sphere. Assuming that there is not a large temperature difference in intermediate-size samples, the heat evolved per unit of volume can be considered approximately constant. From a heat balance and the Fourier law considering an effective thermal conductivity, the following expression can be deduced:

$$d\left[\left(-k_{eff}\frac{dT}{dr_i}\right)4\pi r_i^2\right] \cong k_{ox}\exp\left(-\frac{E_{ox}}{RT_{av}}\right)\Delta H_{ox}\rho_s 4\pi r_i^2 dr_i \tag{9}$$

where r is the radius of the body and T_{av} is an intermediate temperature between T_{outer} (at the outer surface $r_i = r$) and T_{center} (at the center $r_i = 0$).

Integrating, the following equation is obtained

$$T_{outer} - T_{center} \cong r^2\frac{\Delta H_{ox}\rho_S}{6k_{eff}}k_{ox}\exp\left(-\frac{E_{ox}}{RT_{av}}\right) \tag{10}$$

When there is not a negligible resistance to external heat transfer, the $T_{outer} - T_{center}$ difference must be calculated from the observed $T_{ambient} - T_{center}$ deduced. The procedure is the following:

Heat evolved by chemical oxidation = Heat lost to ambient

$$\Delta H_{ox}\rho_S k_{ox}\exp\left(-\frac{E_{ox}}{RT_{av}}\right)\frac{4}{3}\pi r^3 = h4\pi r^2(T_{ambient} - T_{outer}) \tag{11}$$

From Eqs. (10) and (11)

$$1 = \frac{T_{center} - T_{outer}}{\frac{\Delta H_{ox}\rho_S k_{ox}\exp\left(-\frac{E_{ox}}{RT_{av}}\right)}{6k_{eff}}r^2} = \frac{T_{outer} - T_{ambient}}{\frac{\Delta H_{ox}\rho_S k_{ox}\exp\left(-\frac{E_{ox}}{RT_{av}}\right)}{3h}r}$$

$$= \frac{T_{center} - T_{ambient}}{\frac{\Delta H_{ox}\rho_S k_{ox}\exp\left(-\frac{E_{ox}}{RT_{av}}\right)}{6k_{eff}}r^2\left[1 + \frac{2k_{eff}}{h}\right]} \tag{12}$$

From the previous equation

$$T_{center} - T_{outer} = \frac{T_{center} - T_{ambient}}{\left[1 + \frac{2k_{eff}}{hr}\right]} \tag{13}$$

and considering the values of $T_{center} - T_{outer}$, and from Eq. (10):

$$\ln\left[\frac{6(T_{center} - T_{outer})}{r^2}\right] \cong \ln\left[\frac{\Delta H_{ox}\rho_S}{k_{eff}}k_{ox}\right] - \frac{E_{ox}}{RT_{av}} \tag{14}$$

Estimated values of E_{ox}/R and the parameter $\Delta H_{ox}\rho_s k_{ox}/k_{eff}$ can be obtained. With these two parameters, the critical radius r for runaway can be deduced. For values greater than r, runaway will occur; for lower values a steady temperature gradient can be achieved but without runaway.

Two series of runs were performed. Table 7 shows the experimental results of the measured temperatures and the parameters deduced for Series 1 carried out with thermocouples K that recorded the temperatures in units of degrees Celsius. The T_{ave} values have been calculated as $0.8T_{center} + 0.2T_{amb}$ taking into account the exponential variation of the heat evolved with the temperature. The values of 0.8 and 0.2 were selected after a simulation program, but other values, such as 0.5 and 0.5 or 0.9 and 0.1, can be taken and there is no large variation in results. In all cases an approximation is obtained

Fig. 7 shows the variation of the parameters deduced in Table 7.

A new series of runs (Series 2) was carried out with thermocouples K that measured the temperature in units of 0.1 °C, after inter-calibration between them. The effects of radiation on the thermocouple that measured the oven temperature were determined with an aluminum foil sphere with internal pieces of aluminum foil by measuring the temperature inside the sphere and the oven temperature. Table 8 shows the experimental results, which are also plotted in Fig. 7.

Lineal variations can be observed for Series 1 and Series 2. The parameter E_{ox}/R is equal to 11,566 K for Series 1 and 11,654 K for Series 2. The parameter $\Delta H_{ox}\rho_s k_{ox}/k_{eff}$ is equal to exp(35.8090) or 3.562×10^{15}K/m^2 for Series 1 and to exp(35.863) or 3.75×10^{15}K/m^2 for Series 2. In Fig. 7, the deduced variation shown in Figs. 5 and 6 used

Table 7
Experimental temperatures and calculation of parameters. Series 1.

Mass (kg)	Tamb. (°C)	Tcenter (°C)	Tcenter – Tamb. (°C)	r (m)	Tcenter – Touter (°C)	T outer (°C)	Tave. (K)	6*(Tcenter – Touter)/(r^2) (°C/m^2)
0.1563	159.5	164	4.5	0.04691	2.98	161.02	432.95	8117
0.1584	160	165	5	0.04711	3.31	161.69	433.49	8955
0.1543	169.5	179.5	10	0.04670	6.61	172.89	443.33	18,170
0.1603	180	runaway		0.04730				
0.1603	180	runaway		0.04730				
0.1518	175	runaway		0.04645				
0.1818	137	138.5	1.5	0.04933	1.01	137.49	410.25	2488
0.1818	147.5	149.5	2	0.04933	1.35	148.15	420.78	3318
0.1818	158	162.5	4.5	0.04933	3.03	159.47	431.44	7465
0.1818	168	178.5	10.5	0.04933	7.06	171.44	441.84	17,418
0.1813	173.5	runaway		0.04928				

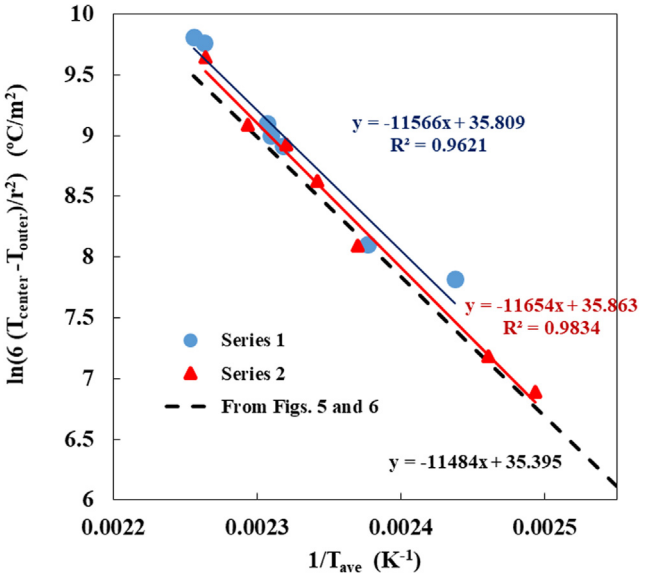

Fig. 7. Variation of $6(T_{center} - T_{outer})/r^2$ vs. $1/T_{ave}$.

in the simulation program also is plotted (E/R equals 11,484 K and the $\Delta H_{ox}\rho_s k_{ox}/k_{eff}$ parameter equals exp(35.395) or $2.354 \times 10^{15} K/m^2$). A similar variation, deduced by the three methods, can be observed. The value of the apparent activation energy is approximately 95–97 kJ/mol, which is a value close to those obtained by different authors, as shown in Tables 2–5. The runaway runs were tested by the simulation program.

4. Extrapolation of data

In order to analyze the influence of the vapor sorption of the spontaneous combustion, several simulations have been carried out considering large spheres, 3 m diameter, 5112 kg. Equivalent spheres with the same volume than piles of different form can be considered as an approximation to analyze the physical/chemical processes involved.

The parameters considered were the same as those previous used in the runs explained above: mass transfer coefficient K_x 0.00831 kg water/(s m^2 Δ(kg water/kg dry air)); internal diffusion coefficient D_{eff} $1.565 \times 10^{-7} m^2/s$; sorption equilibria: moisture content (kg water/kg d.s.) = 5431*(temperature in °C)$^{-2.669}$; heat transfer coefficient 11.5 J/s m^2 K; internal effective thermal conductivity 0.120 J/s m °C; enthalpy of oxidation 5.241×10^6 J/kg; pre-exponential kinetic factor $1.559 \times 10^5\ s^{-1}$; E/R 11,484 K.

The influence of external heat transfer is practically insignificant, so the temperature of the outer element is practically equal to the ambient temperature. The critical temperature for runaway considering only chemical oxidation is 78.4 °C, deduced from Eq. (1).

Fig. 8 shows the simulated results at different initial temperatures coinciding with the constant ambient temperature considering that the initial solid is dry, with and without vapor sorption:

- In the cases (a) and (b) with vapor sorption, there is runaway despite the fact that the ambient and initial temperatures, 75 and 60 °C, respectively, are lower than the critical temperature of 78.4 °C. These ambient temperatures of 75 and 60 °C could be reached by biological oxidation in the first stage of temperature increase, but then, during the chemical oxidation stage, the drying must be small so the heat evolved by the chemical oxidation serves to increase the temperature and not for water vaporization.
- In the case (c) without vapor sorption, there is no runaway because the ambient temperature 75 °C is lower than the critical 78.4 °C, while in case (d), there is runaway because the ambient temperature of 80 °C is higher than the critical temperature of 78.4 °C, but after a long period of 82.5 days.

Fig. 9 shows the simulated results for a spherical body of 4 m diameter, with the same parameters indicated in the cases of Fig. 8, but with the sorption equilibrium: moisture content (kg water/kg d.s.) = 0.3444 exp(–0.02624 *temperature in °C), presented in Fig. 4a. The critical temperature for runaway in this case is 74.8 °C, lower than for the cases of the spherical body with 3 m diameter. For case (a) without vapor sorption, the induction time for runaway is 39.3 days for an ambient temperature of 80 °C, while in the case of vapor sorption, the runway takes place at a temperature of 45 °C, lower than the critical temperature and with an induction time of 27.1 days.

Tables 2–5 show some results of the induction time proposed by researchers for low ambient temperatures considering only, in most cases, chemical oxidation, and with very long periods, of months to several years, to reach runaway.

It can be deduced that vapor sorption increases the initial temperature of the body with a double effect: it exceeds the critical temperature toward runaway and increases the oxidation rate due to the increase in temperature. This is in agreement with the conclusions obtained by Lohrer et al. [16].

The experimental determination of the critical temperature for runaway is not easy, because with a temperature slightly below the critical temperature there is no runaway, but with a temperature slightly higher than the critical temperature, there is runaway but after a very long period.

According to the theory criticality of Frank-Kamenetskii [6,7], it is not possible to calculate the induction time for the runaway. There are many authors who have carried out extrapolation of the experimental data, both for the critical temperature and for the induction time, by log–log variation and taking into account the V/A ratio or a characteristic length, as shown in Tables 2–5.

For adiabatic experiments, the adiabatic induction period t_{ad} to the runaway can be calculated approximately as [8]:

$$\frac{1}{t_{ad}} = \frac{\Delta H_{ox} k_{ox}}{C_p} \frac{E_{ox}}{RT_o^2} \exp\left(-\frac{E_{ox}}{RT_o}\right) \quad (15)$$

where $T_o$is the initial temperature (K) of the body. The induction periods for the runaway runs according to the Frank-Kamenetskii theory of criticality are greater than those calculated by Eq. (15) due to the heat loss from the material to the ambient. In both cases, the period to raise

Table 8
Experimental temperatures and calculation of parameters. Series 2.

Mass (kg)	Tamb. (°C)	Tcenter (°C)	Tcenter – Tamb. (°C)	r (m)	Tcenter–Touter (°C)	T outer (°C)	Tave. (K)	6*(Tcenter – Touter)/(r^2) (°C/m^2)
0.1852	122.90	123.10	0.20	0.0496	0.13	122.97	396.06	328
0.1852	127.90	128.50	0.60	0.0496	0.40	128.10	401.09	985
0.1852	133.20	134.00	0.80	0.0496	0.54	133.46	406.40	1313
0.1852	148.70	150.70	2.00	0.0496	1.35	149.35	421.98	3283
0.1852	153.60	157.00	3.40	0.0496	2.29	154.71	426.97	5582
0.1852	157.60	162.20	4.60	0.0496	3.10	159.10	431.05	7552
0.1852	162.50	167.90	5.40	0.0496	3.64	164.26	436.00	8865
0.1852	167.90	177.30	9.40	0.0496	6.34	170.96	441.66	15,432

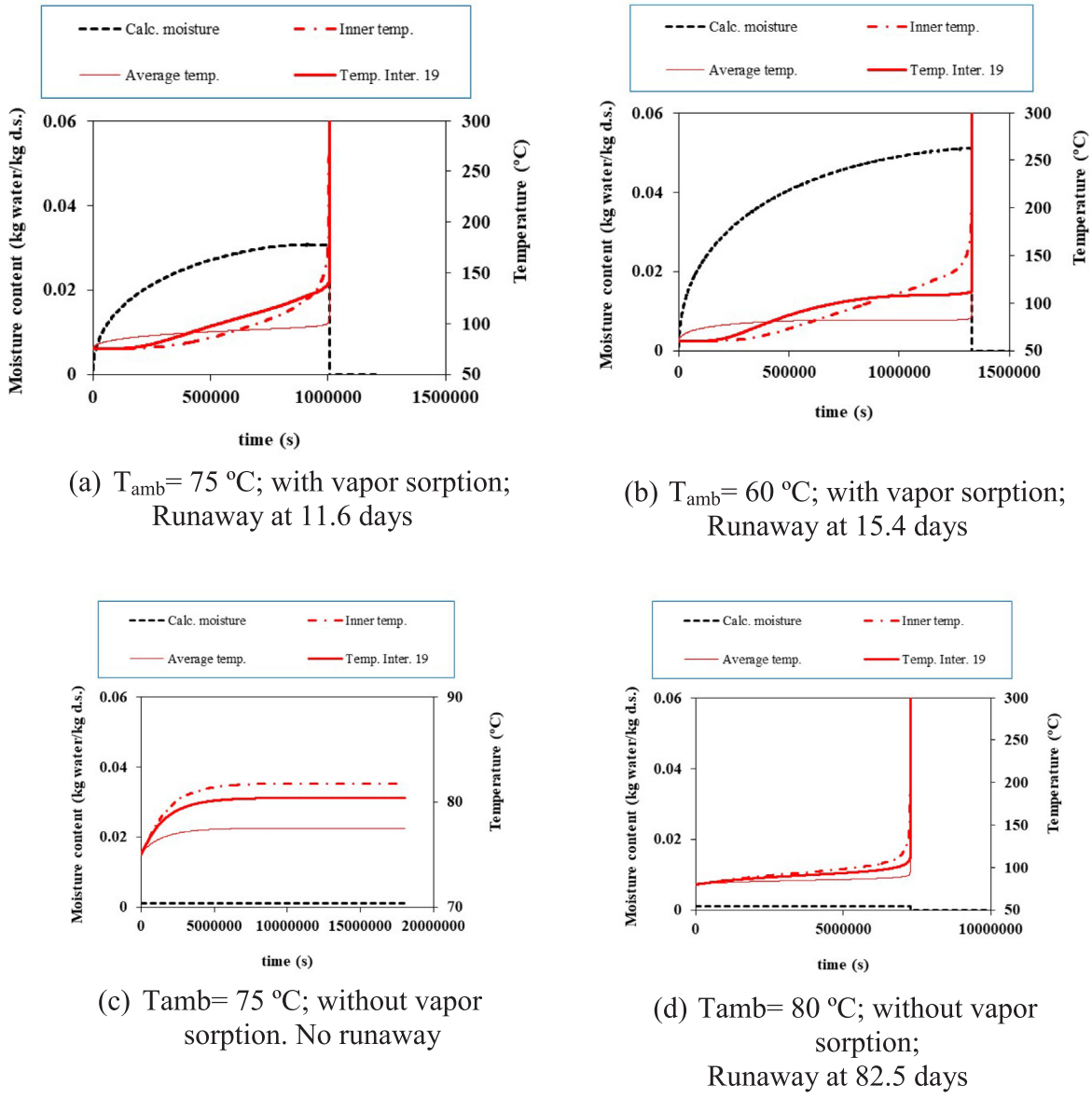

Fig. 8. Simulation results considering a 3 m diameter spherical body (critical temperature for runaway 78.4 °C).

the temperature from room temperature to, for example, 90–110 °C is very long because the oxidation rate is very small. Body size does not affect an adiabatic run. For a run with internal heat transfer to ambient, as in the Frank-Kamanetskii model, in general the lower the critical temperature, the greater the body, the longer the induction time to runaway for temperatures 2 ó 5 °C higher than the critical temperature (note that at the critical temperature the runaway would take place after infinite time).

In cases where there is aerobic fermentation that can increase the temperature from room temperature to 60–75 °C and the vaporization of water takes place very slowly, the chemical oxidation rate can be sufficient for runaway. The metabolism of the cells releases heat to 80 °C, although the cells die between 50 and 60 °C [57]. Fungi can grow on wood with low moisture levels (around 10% with humid air) [58].

In other cases, with very dry material, water vapor sorption can also increase the temperature to 30 or 40 °C above room temperature, and then chemical oxidation may be important. Water vapor can come from humid air, biological digestion that generates water vapor, chimneys, smoke from machinery or other processes.

The combination of aerobic digestion, drying without a large temperature decrease, vapor sorption and chemical oxidation increases the possibility of runaway The analysis presented can be applied to other wastes. Testing of the simulation program should be done in a large reactor and would require a long period of time, and this would be the goal of another research program.

5. Conclusions

Sorption of water vapor was studied in an oven with an external balance, obtaining a decreasing variation in moisture content with oven temperature. A simulation program was also developed for the analysis of experimental data. From the run carried out with a sample of spherical shape wrapped in perforated aluminum foil to study the kinetics, a peak experimental increase in temperature of 26 °C was observed.

The variation of moisture content was discussed and simulated satisfactorily, assuming that water vapor sorption take place within the sample, the internal diffusion follows Fick‘s law and that the moisture content in each layer cannot exceed the limit of moisture deduced previously and corresponding to equilibrium.

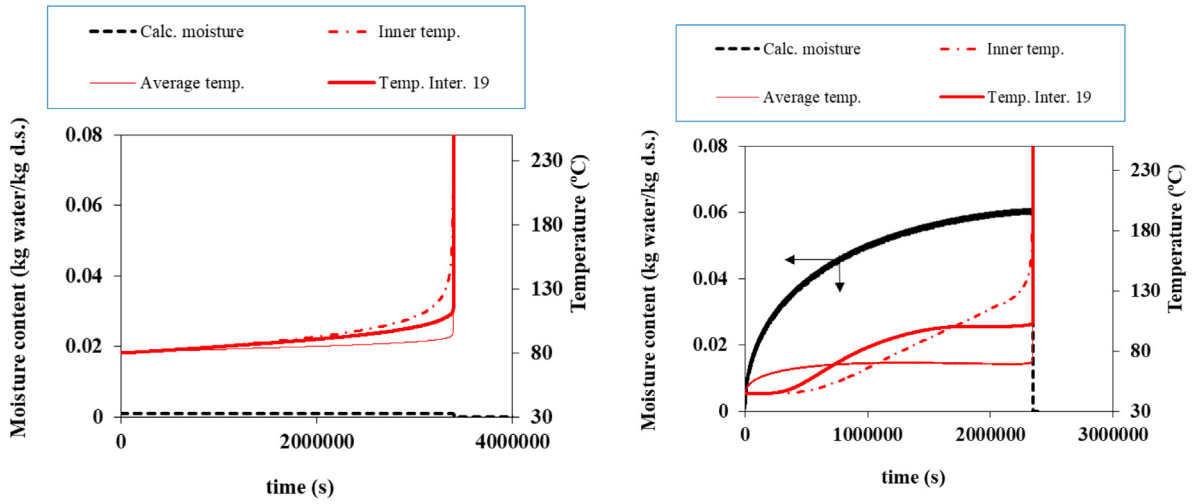

(a) T_{amb}= 80 ºC; without vapor sorption; Runaway at 39.3 days

(b) T_{amb}= 45 ºC; with vapor sorption; Runaway at 27.1 days

Fig. 9. Simulation results considering a 4 m diameter spherical body (Critical temperature for runaway 74.8 ˚C).

The kinetic constants for chemical oxidation were deduced by two procedures: one by the rate of weight loss and the other by determination of the temperature difference between the inside and outside of a spherical sample wrapped in perforated foil. A numerical program was used to simulate an actual run.

In addition, a numerical program was used to simulate the runaway of a spherical body at different temperatures, with and without vapor sorption. It was deduced that vapor sorption can have a double effect: increasing the temperature toward runaway and increasing the rate of oxidation due to the increase in temperature. From the simulation program it can be deduced that runaway can be obtained after 27.1 days with an outside temperature of 45 ˚C prior to water vapor sorption.

Analysis and discussion of de data shows that there is a risk of self-combustion in large amounts of material and under some conditions, including water vapor sorption.

Declaration of Competing Interest

The authors declare that they have no known competing financial interests or personal relationships that could have appeared to influence the work reported in this paper.

Acknowledgement

The collaboration of Daniel Agustín Ortiz de la Morena and Ana Isabel Moreno Caballero for their help in the implementation of the equipment and Alicia Font Escamilla for her help in correcting the work are thanked. Funding is from the University of Alicante. The support of the research funds of the University of Alicante is appreciated.

References

[1] Fu ZM, Koseki H, Iwata Y. Investigation on spontaneous ignition of two kinds of organic material with water. Thermochim Acta 2006;440:68–74.
[2] Hill CAS, Norton A, Newman G. The Water Vapor Sorption Behavior of Natural Fibers. J Appl Polym Sci 2009;112:1524–37.
[3] Guo X, Wu YQ, Xie XF. Water vapor sorption properties of cellulose nanocrystals and nanofibers using dynamic vapor sorption apparatus. Sci Rep-Uk 2017;7.
[4] Sghaier K, Peczalski R, Bagane M. Water sorption equilibria and kinetics of henna leaves. Heat Mass Transfer 2018;54:1545–54.
[5] Murr A, Lackner R. Analysis on the influence of grain size and grain layer thickness on the sorption kinetics of grained wood at low relative humidity with the use of water vapour sorption experiments. Wood Sci Technol 2018;52:753–76.
[6] P.C. Bowes, Application of the Theory of Thermal Explosion to the Self-Heating and Ignition of Organic Materials, in: F.R.N.N. 867 (Ed.), 1971.
[7] B.F. Gray, Spontaneous-Combustion and Self-Heating, in: M. Hurley (Ed.) SFPE Handbook of Fire Protection Engineering, Springer, New York, 2016.
[8] Schmidt M, Wanke C, Krause U. Determination of Measurement Uncertainties in Adiabatic Hot-Storage Experiments for Reactive Dusts. Chem Eng Technol 2013;36:1764–72.
[9] Chen XD, Chong LV. Several important issues related to the crossing-point temperature (CPT) method for measuring self-ignition kinetics of combustible solids. Process Saf Environ 1998;76:90–3.
[10] Chong LV, Chen XD, Mackereth AR. Effect of ageing and composition on the ignition tendency of dairy powders. J Food Eng 1999;39:269–76.
[11] A.C. Smith, Y. Miron, C.P. Lazzara, Large-scale studies of spontaneous combustion of coal, in: U.S.B.o. Mines (Ed.), Spokane Research Center, 1991.
[12] Vance WE, Chen XD, Scott SC. The rate of temperature rise of a subbituminous coal during spontaneous combustion in an adiabatic device: The effect of moisture content and drying methods. Combust Flame 1996;106:261–70.
[13] Ibarra JV, Miranda JL. Detection of weathering in stockpiled coals by Fourier transform infrared spectroscopy. Vib Spectrosc 1996;10:311–8.
[14] Nugroho YS, McIntosh AC, Gibbs BM. On the prediction of thermal runaway of coal piles of differing dimension by using a correlation between heat release and activation energy. P Combust Inst 2000;28:2321–7.
[15] Wang H, Dlugogorski BZ, Kennedy EM. Analysis of the mechanism of the low-temperature oxidation of coal. Combust Flame 2003;134:107–17.
[16] Lohrer C, Krause U, Steinbach J. Self-ignition of combustible bulk materials under various ambient conditions. Process Saf Environ 2005;83:145–50.
[17] Lohrer C, Schmidt A, Krause U. A study on the influence of liquid water and water vapour on the self-ignition of lignite coal-experiments and numerical simulations. J Loss Prevent Proc 2005;18:167–77.
[18] Butakova VI, Posokhov YM, Popov VK. Identification of Active Centers in Coal Oxidation by Molecular Simulation. Coke Chem 2011;54.
[19] Wu DJ, Huang XY, Norman F, Verplaetsen F, Berghmans J, Van den Bulck E. Experimental investigation on the self-ignition behaviour of coal dust accumulations in oxy-fuel combustion system. Fuel 2015;160:245–54.
[20] Wu DJ, Norman F, Schmidt M, Vanierschot M, Verplaetsen F, Berghmans J, et al. Numerical investigation on the self-ignition behaviour of coal dust accumulations: The roles of oxygen, diluent gas and dust volume. Fuel 2017;188:500–10.
[21] Wu DJ, Schmidt M, Huang XY, Verplaetsen F. Self-ignition and smoldering characteristics of coal dust accumulations in O-2/N-2 and O-2/CO2 atmospheres. P Combust Inst 2017;36:3195–202.
[22] X. Wang, Y. Luo, Study on correlation of quantified coal rank with self-heating temperature, Mining Enginnering, November (2015) 54-60.
[23] Kim CJ, Sohn CH. Effects of wind barrier design and closed coal storage on spontaneous ignition of coal stockpiles. J Loss Prevent Proc 2016;40:529–36.
[24] Kaminsky VA, Obvintseva NY, Epshtein SA. The estimation of the kinetic parameters of low-temperature coal oxidation. Aims Energy 2017;5:163–72.
[25] Lin Q, Wang SG, Liang YT, Song SL, Ren TX. Analytical prediction of coal spontaneous combustion tendency: Velocity range with high possibility of self-ignition. Fuel Process Technol 2017;159:38–47.
[26] Lu W, Cao YJ, Huang ZA, Tien JC, Qin BT. Study on adiabatic oxidation characters of coal with applying a constant temperature difference to guide the oxidation of coal with temperature rising. Energ Fuel 2017;31:882–90.
[27] Restuccia F, Huang XY, Rein G. Self-ignition of natural fuels: Can wildfires of carbon-rich soil start by self-heating? Fire Safety J 2017;91:828–34.

[28] Wang YJ, Zhang XM, Sugai Y, Sasaki K. Determination of critical self-ignition temperature of low-rank coal using a 1 m wire-mesh basket and extrapolation to industrial coal piles. Energ Fuel 2017;31:6700–10.
[29] m. Pólka, Analysis of suscelītibility of peat on its spontaneous heating and self-ignition properties, MATEC Web of Conferences, 247 (2018).
[30] Yuan H, Restuccia F, Richter F, Rein G. A computational model to simulate self-heating ignition across scales, configurations, and coal origins. Fuel 2019;236:1100–9.
[31] Janes A, Carson D, Accorsi A, Chaineaux J, Tribouilloy B, Morainvillers D. Correlation between self-ignition of a dust layer on a hot surface and in baskets in an oven. J Hazard Mater 2008;159:528–35.
[32] Krause U, Schmidt M, Ferrero F. Investigation of the development of conflagration of solid material via analysis of coupled heat, mass and momentum transport. Chem Eng Technol 2009;32:292–305.
[33] Garcia-Torrent J, Ramirez-Gomez A, Querol-Aragon E, Grima-Olmedo C, Medic-Pejic L. Determination of the risk of self-ignition of coals and biomass materials. J Hazard Mater 2012;213:230–5.
[34] Veznikova H, Perdochova M, Bernatik A, Binkau B. Safe storage of selected fuels with regard to their tendency to spontaneous combustion. J Loss Prevent Proc 2014;29:295–9.
[35] Binkau B, Wanke C, Krause U. Influence of inert materials on the self-ignition of flammable dusts. J Loss Prevent Proc 2015;36:337–44.
[36] van Graan MaBJR. Evaluation of a TGA Method to predict the ignition temperature and spontaneous combustion propensity of coals of different rank. International Conference on Advances in Science, Engineering, Technology and Natural Resources (ICASETNR-16). Parys: South Africa; 2016.
[37] Magalhaes D, Kazanc F, Ferreira A, Rabacal M, Costa M. Ignition behavior of Turkish biomass and lignite fuels at low and high heating rates. Fuel 2017;207:154–64.
[38] Fernandez-Anez N, Garcia-Torrent J. Influence of particle size and density on the hot surface ignition of solid fuel layers. Fire Technol 2019;55:175–91.
[39] Sidhu HS, Nelson MI, Luangwilai T, Chen XD. Mathematical modelling of the self-heating process in compost piles. Chemical Product and Process Modeling 2007;2:8.
[40] Moraga NO, Corvalan F, Escudey M, Arias A, Zambra CE. Unsteady 2D coupled heat and mass transfer in porous media with biological and chemical heat generations. Int J Heat Mass Tran 2009;52:5841–8.
[41] Pejic LM, Anez NF, Torrent JG, Ramirez-Gomez A. Determination of spontaneous combustion of thermally dried sewage sludge. J Loss Prevent Proc 2015;36:354–9.
[42] Torrent JG, Ramirez-Gomez A, Fernandez-Anez N, Pejic LM, Tascon A. Influence of the composition of solid biomass in the flammability and susceptibility to spontaneous combustion. Fuel 2016;184:503–11.
[43] Putranto A, Chen XD. A new model to predict diffusive self-heating during composting incorporating the reaction engineering approach (REA) framework. Bioresource Technol 2017;232:211–21.
[44] Diaz E, Pintado L, Faba L, Ordonez S, Gonzalez-LaFuente JM. Effect of sewage sludge composition on the susceptibility to spontaneous combustion. J Hazard Mater 2019;361:267–72.
[45] Ferrero F, Lohrer C, Schmidt BM, Noll M, Malow M. A mathematical model to predict the heating-up of large-scale wood piles. J Loss Prevent Proc 2009;22:439–48.
[46] Moqbel S, Reinhart D, Chen RH. Factors influencing spontaneous combustion of solid waste. Waste Manage 2010;30:1600–7.
[47] Ramirez A, Garcia-Torrent J, Tascon A. Experimental determination of self-heating and self-ignition risks associated with the dusts of agricultural materials commonly stored in silos. J Hazard Mater 2010;175:920–7.
[48] Torrent JG, Anez NF, Pejic LM, Mateos LM. Assessment of self-ignition risks of solid biofuels by thermal analysis. Fuel 2015;143:484–91.
[49] Murasawa N, Koseki H. Investigation of heat generation from biomass fuels. Energies 2015;8:5143–58.
[50] Jones JM, Saddawi A, Dooley B, Mitchell EJS, Werner J, Waldron DJ, et al. Low temperature ignition of biomass. Fuel Process Technol 2015;134:372–7.
[51] Ronda A, Della Zassa M, Biasin A, Martin-Lara MA, Canu P. Experimental investigation on the smouldering of pine bark. Fuel 2017;193:81–94.
[52] Sedlmayer I, Arshadi M, Haslinger W, Hofbauer H, Larsson I, Lonnermark A, et al. Determination of off-gassing and self-heating potential of wood pellets - Method comparison and correlation analysis. Fuel 2018;234:894–903.
[53] Schwarzer L, Sarossy Z, Jensen PA, Glarborg P, Karlstrom O, Holm JK, et al. Kinetic parameters for biomass under self-ignition conditions: Low-temperature oxidation and pyrolysis. Energ Fuel 2019;33:8606–19.
[54] Dupont C, Chiriac R, Gauthier G, Toche F. Heat capacity measurements of various biomass types and pyrolysis residues. Fuel 2014;115:644–51.
[55] Font R, Gomez-Rico MF, Fullana A. Skin effect in the heat and mass transfer model for sewage sludge drying. Sep Purif Technol 2011;77:146–61.
[56] King CJ. Rates of moisture sorption and desorption in porous dried foodstuffs. Food Technol-Chicago 1968;22. 509-&.
[57] Kubler H. Heat release in thermally disintegrating wood. Wood Fiber Sci 1982;14:166–77.
[58] Krigstin S, Wetzel S. A review of mechanisms responsible for changes to stored woody biomass fuels. Fuel 2016;175:75–86.